JOURNAL OF SPACECRAFT AND ROCKETS
Vol. 33, No. 5, September–October 1996

Interaction of Solid-Rocket Exhaust with the Atmosphere

David J. Knecht,* Charles P. Pike,† and Edmond Murad‡
U.S. Air Force Phillips Laboratory, Hanscom Air Force Base, Massachusetts 01731-3010
and
David L. A. Rall§
PhotoMetrics, Inc., Woburn, Massachusetts 01801-2067

Photometrically calibrated, ground-based, wide-band images were recently obtained for the exhaust trail of an aluminized solid-rocket motor of 10,000-kgf thrust operating and smoldering near 110 km. These observations were made in the visible and near infrared using an intensified video camera mounted on the acquisition telescope of the 1.6-m telescope at the U.S. Air Force Maui Optical Site. The burn-associated luminous volume expands within a few frames to about 1 km transverse to the trajectory, with most of the emission occurring near its stationary edges. Its initial lifetime, determined from individual as well as sequential images, is 13 ± 3 s. This spatial distribution and persistence show that the emission is not due to thermal radiation from or catalyzed by micrometer-scale Al_2O_3 exhaust particles. Assuming that the chemiluminescence is due to the reaction of ambient atomic oxygen with the combustion products of the exhaust, the data lead to a depletion-rate coefficient of about 10^{-12} cm^3 molecule^{-1} s^{-1}. We suggest that a key step in producing the emission is due to Al-containing complexes reacting exothermally with O atoms in the upper atmosphere. The visible-light-emitting species is likely to be an electronically excited state of AlO_2 or AlO. Analysis of the hydrodynamic development of the radiating volumes leads to their scaling to other solid-rocket thrusts and altitudes.

Nomenclature

E = energy released by explosion, J
k = scaling factor
P = pressure of ambient atmosphere, N/m^2
R = radius of exhaust trail, m
v = collision velocity, m/s
Λ = energy released per unit trail length, J/m
μ = reduced mass, kg

Subscripts

b = burn
s = smolder

Introduction

WE analyze in this report a ground-based observation of self-luminous exhaust trails produced by the second- and third-stage solid-propellant motors of a rocket whose altitude remained near 110 km during the burns. These measurements were made in support of the STRYPI-XI Bowshock Experiment, but the results reported here are unrelated to the principal goals of that experiment. The interaction of its exhaust with the atmosphere was observed with instrumentation on telescopes of a nearby observatory. This experiment followed a series in which all previous observations had been directed at engine-exhaust plumes of the Space Shuttle, which have been seen to interact with the atmosphere to produce a luminous volume having dimensions of several kilometers and a persistence, for at least one component, of many seconds.[1,2] Space Shuttle engines use a liquid fuel and oxidizer (monomethyl hydrazine and N_2O_4), and the products of combustion are gaseous species (see, for example, Pickett et al.[3]). Engines fired in the ram direction afford collision velocities between exhaust products and atmosphere as high as 11.2 km/s (from an orbital velocity of 7.7 km/s plus the exhaust velocity of 3.5 km/s), which are high enough to permit endoergic chemical reactions in which potential barriers must be overcome; the available energy in the center-of-mass system is $\mu v^2/2$. These Shuttle experiments were all done at altitudes near 300 km, where the interaction between engine exhaust and atmosphere proceeds primarily through two-body collisions. The exhaust plume resembles a piston that compresses and accelerates the atmosphere ahead of it, causing energetic collisions that form $O(^1D)$, which then radiates in a luminous cloud well ahead of the Shuttle.

The present experiment, by contrast, was conducted at an altitude near 110 km, where the interaction is much more complex; the dynamics of the combustion makes it likely that condensation of minor constituents plays an important role in both the interaction and the eventual dissipation of the products. The chemical composition of the exhaust is simpler for the Shuttle than for the solid motor, though there are some similarities in the minor constituents. However, the most important difference is probably that the collision energy is now too low to play a significant role. Since the rocket velocity was limited to the range from nearly zero to 2.5 km/s (into ram) and the exhaust velocity was only about 1.5 km/s in the opposite (wake) direction, the collision velocity never exceeded 1.5 km/s, and the collision energy was never more than 2% of that available in the Shuttle exhaust.

The ignition of a solid fuel, the first step in the combustion, has been treated both theoretically and experimentally, as discussed in detail by Hermance.[4] The dynamics of the combustion following ignition has been discussed in detail by Price.[5] For aluminized solid propellants, the major end products are Al_2O_3, CO, H_2, N_2, H_2O, and HCl; in addition, there are small amounts of free-radical intermediates,[6,7] such as OH, AlO, Al_2O, AlO_2, and AlCl. The exhaust is believed to consist of Al_2O_3 droplets surrounded by various combustion products that depend on distance from the release point. The role of free-radical intermediates in the production of persistent visible radiation, which we will address, has not previously been considered, nor has the role of gas-phase reactions in the combustion and the transport of combustion products. This experiment sought to obtain phenomenological data that might bear on these questions. Most previous studies have been concerned with measurement of the exhaust composition. By contrast, this report focuses primarily on the dynamics of the exhaust and the observation of persistent self-luminous trails.

Received March 20, 1995; revision received April 19, 1996; accepted for publication April 29, 1996.

*Physicist, Ionospheric Interactions Branch, 29 Randolph Road.
†Director, Ionospheric Effects Division, 29 Randolph Road.
‡Chemist, Ionospheric Interactions Branch, 29 Randolph Road.
§Staff Scientist, 4 Arrow Drive.

Experiment

The second- and third-stage burns of a three-stage STRYPI rocket, launched on Feb. 18, 1991, from Kauai, Hawaii (22.07°N, 159.75°W), were observed through telescopes of the U.S. Air Force Maui Optical Station (AMOS) at 3-km altitude on Maui, Hawaii (20.71°N, 156.26°W). Figure 1 is a sketch (looking south, not to scale) of the viewing geometry. The first stage, at an azimuth heading of about 200 deg (southwest), lifted the rocket to about 105 km, where the upper stages were reoriented to be nearly horizontal, with an azimuth heading of about 140 deg (southeast). The second stage, a solid-composite Antares II motor (Hercules X259A2), accelerated the rocket over a 30-km horizontal distance with a gain in altitude of only 6 km. Velocities at the start and end of its burn were 0.30 and 2.55 km/s, respectively. After burnout the rocket coasted, but the motor smoldered, producing a small residual thrust that persisted through third-stage separation and ignition at 119-km altitude. Here the rocket was aimed slightly below horizontal to bring it deeper into the atmosphere; the third stage, a Star-27 motor (Thiokol TE-M-616), accelerated the rocket over a 152-km distance with an 8-km loss in altitude. The closest approach to AMOS occurred very near the time of third-stage burnout, when the velocity had reached about 5.1 km/s. The trajectory and viewing geometry are described further in Fig. 1 and Table 1.

At AMOS, two main telescopes and their acquisition telescope systems were used to observe the rocket, and images having various magnifications and spectral responses were recorded. However, only images from the MOTIF Acquisition Telescope System (MATS) will be analyzed and discussed here. The MATS focal plane is an intensified visible-wavelength video camera (ISIT photodetector)[1,8]; it has a nominal (uncharacterized) S-20 response, a 3-deg field of view, and a frame rate of 30 s^{-1}.

The MATS images show two dominant features: 1) an extremely bright exhaust during motor burns and 2) a persistent luminous trail deposited along the trajectory behind the rocket. The bright exhaust will not be considered here. Its spectrum was measured in a separate AMOS experiment and found to match a graybody spectrum calculated for the temperature of the condensed exhaust of the aluminum fuel; in much less than 1 s these particles are too cool to radiate appreciably at visible wavelengths, so the observed length of this bright volume was only about 75 m. The subject of this report is the persisting visible trail that was seen, without illumination by sun or moon, during both the burn and the subsequent coast. Selected MATS image frames at various times after ignition are shown Fig. 2.

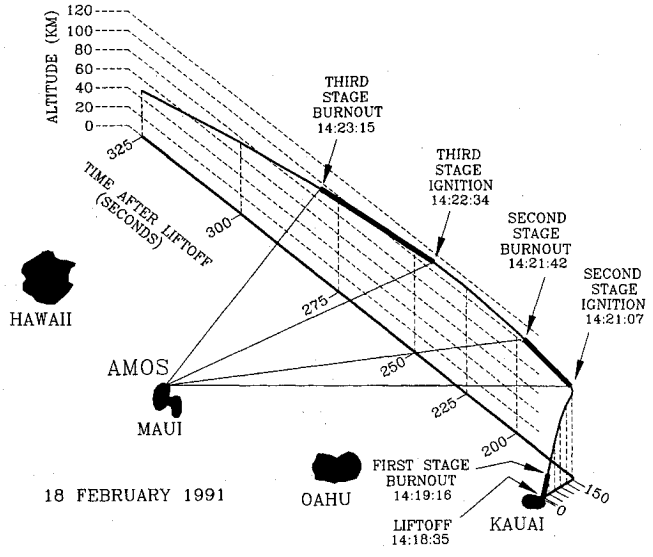

Fig. 1 Schematic view of the rocket trajectory, Hawaiian Islands, and AMOS observatory.

Table 1 STRYPI-XI trajectory parameters

Time, s	Range,[a] km	Altitude, km	Elev.,[a] deg	Azim.,[a] deg	Speed, km/s	Aspect, deg
140.0	476.4	102.4	8.1	292.2	0.371	50.2
150.0	457.6	104.4	9.4	290.0	0.317	43.1
155.1[b]	448.4	105.2	10.1	290.0	0.310	38.9
160.0	439.2	105.8	10.7	289.2	0.391	35.1
165.0	430.1	106.1	11.4	288.4	0.618	34.4
170.0	421.2	106.7	12.1	287.5	0.904	35.1
175.0	412.3	107.5	12.7	286.6	1.250	35.4
180.0	403.5	108.2	13.4	285.6	1.618	36.8
185.0	394.8	109.3	14.0	284.5	2.050	37.8
190.5[c]	386.2	110.9	14.6	283.6	2.567	39.3
195.0	377.7	112.5	15.3	282.5	2.634	40.7
205.0[d]	361.1	115.3	16.5	280.0	2.621	43.7
215.0	344.9	117.3	17.6	277.4	2.610	47.0
225.0	329.4	118.2	18.7	274.4	2.600	50.9
235.0	314.5	118.8	19.6	271.1	2.606	55.2
239.0[b]	308.8	118.8	19.9	269.7	2.616	57.7
245.0[c]	300.4	118.8	20.4	267.4	2.836	61.6

[a]Range, elevation, and azimuth measured from AMOS.
[b]Time of engine ignition.
[c]Time of engine burnout.
[d]Time of smolder shown in Fig. 12.

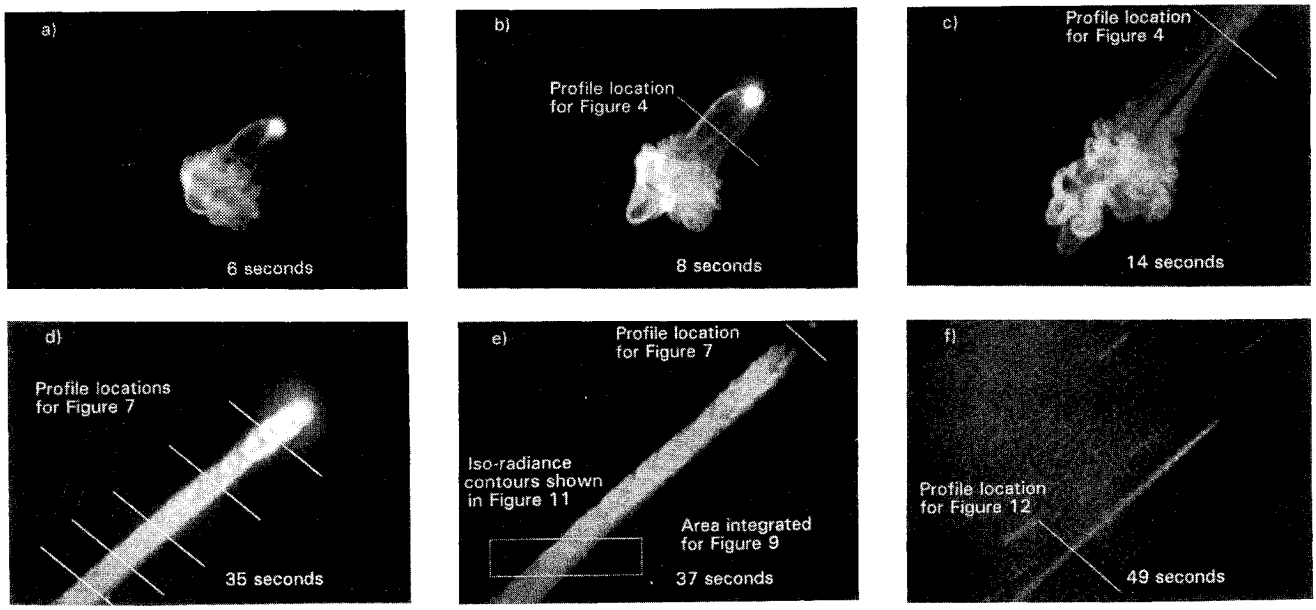

Fig. 2 Selected video images of the luminous trail left by the Antares II rocket motor.

The rocket (the bright disk in frames a, b, and d) is approaching the camera, so the frame diagonal changes from 23.5 km at ignition to 18.0 km in panel f. The local horizontal is found by rotating the bottom edge of the frame clockwise by 75–83 deg over this interval; an observer standing at AMOS, facing the rocket, would see it move up and to his left (see Fig. 1). The telescope was motionless until 16 s after ignition (frames a–c), after which it tracked the rocket body through third-stage burnout. Because the trail is more than 10 km in length, its structure is easily observed within the 50-mrad MATS field of view but not in the typically 1-mrad fields of view of most other AMOS cameras. Traces (and a box) drawn on Fig. 2 show the locations of radiance measurements shown later in Figs. 4, 7, and 10–12.

The engine burns were also observed by the LACE satellite overhead[9] and instruments in the STRYPI nose cone.[10,11] Only one space-based instrument, an intensified camera on LACE, sensitive between 250 and 450 nm, detected the persistent trail (but not the smolder) discussed here. The LACE images show about the same dimensions, a similar rate of decay, and a maximum surface brightness roughly one-fourth of that reported here for longer wavelengths.

Overview of the Telescope Images

Figure 2 shows selected video frames from the MATS camera during the second-stage burn and subsequent coast period. The rocket is approaching AMOS; the decrease in range causes the distance (at the rocket) represented by the frame diagonal to decrease by 14% during the 35-s Antares burn. The angle between the exhaust direction and the line of sight to AMOS was approximately 146 deg at second-stage ignition and decreased to 90 deg only around the time of third-stage burnout, so the line of sight did not permit viewing directly into the combustion chamber. However, the vehicle was too small to obscure the hot exhaust volume, which was bright enough to saturate the camera, and its image is highly bloomed. The hot exhaust will not be discussed further.

The glowing trail began, at motor ignition, with a bright patch or cloud that resembled a puff of smoke. This cloud, ejected backward from a forward-moving rocket, appeared to hang nearly motionless in space. The luminous emission came mostly from the outer edge, as evidenced by limb brightening. The surface radiance varied by a factor of 3, and no characteristic cell size was apparent. The cloud appeared to comprise two overlapping volumes, and the subsequent trail appeared to comprise two components lying side by side. We presume this to result from the asymmetric internal mechanical shape of the motor; four slots molded into the propellant (in planes containing the long axis) are spaced with separations of 60, 120, 60, and 120 deg. The cloud expanded slowly, its maximum width increasing by 1.5 km (from 3.8 to 5.3 km) in the interval between 2 and 16 s after ignition. Also during this period, a small jet or "finger" emerged from this cloud in the wake direction, with a velocity of 300 ± 50 m/s, reaching a diameter of 1 km and a length of 5 km, and limb-brightened like the original cloud. The accidental lingering of the telescope on this cloud afforded 16 s of observation time rather than the 6 s (or less) for which the subsequent trail remained within view.

The burning motor then continued to lay down a glowing exhaust trail characterized by laminar flow. It is bifurcated near the nozzle into two components that quickly merge into a single cylindrically symmetric form, which initially expanded radially at about 3–4 km/s but stopped when the diameter had reached about 1 km. The trail is not perfectly uniform; macroscopic turbulence features are observed that have velocities of hundreds of meters per second in the wake direction. There is very little variation of intensity with distance from the nozzle. Movement of the trail transverse to the line of sight indicates that the trail is carried by upper atmospheric winds.

The second-stage burn was followed by a 24-s coast before the two stages separated and another 24-s pause before the third stage fired. During all of this time the Antares motor smoldered and continued to lay down a visible trail, but its intensity was lower by a factor of 10 to 100. Its width (cylindrical diameter) was much smaller but continued to expand as long as it remained within view. This width also shows a regular variation with distance from the nozzle, which probably results from a combination of an asymmetric exhaust stream and the spin rate (about 1.7 s^{-1}) of the motor. The smoldering motor continued to produce an appreciable thrust; within 11 s of separation from the third stage it had overcome the separation velocity (imparted by mechanical springs) and unexpectedly (but not catastrophically) collided with the third stage.

Data Reduction

The MATS camera is a target-acquisition tool, not a scientific instrument; it is not radiometrically calibrated and is not amenable to calibration after the fact. While tracking a burning rocket, its gain is adjusted occasionally in response to large changes in brightness but usually remains fixed during long intervals between these changes. During these intervals, the brightness scale for the images can be estimated by comparison with known stars that pass through the field. To compensate for such gain adjustments during thruster operation, we calibrated several sets of frames by relating, for each of several star images, the integrated brightness and point spread to the known magnitude and spectral class. Stars seen in the frames were identified from standard charts and the SkyMap listing.[12] This method automatically accounts for the effect of atmospheric transmission.[1,8] We will use the term relative intensity for the value of the digitized (to 8-bit accuracy) video signal with the dark-background baseline subtracted. The absolute radiant intensities quoted in later figures include only that part of the spectrum to which the camera is sensitive (380–670 nm). Their estimated overall uncertainty is about a factor of 3, as the stars and the trail presumably have different spectral distributions.

We determined the time dependence of the relative intensity of the trail after deposition by measuring its decrease both in successive video frames at a fixed position and in a single frame at a series of down-trail positions corresponding to successive times after passage of the thruster. The first method examines a single altitude, while the second examines a range of altitudes. To relate apparent brightness to radiance per unit mass, we need to know how the density of exhaust gases varies within the trail. Since the velocity of the exhaust stream relative to the rocket and the rate of mass deposition into the stream remain roughly constant, the density within the trail will vary only if the trail expands transversely (perpendicular to the velocity vector) or the rocket velocity changes. There is no appreciable transverse expansion (see Fig. 2) after the initial expansion to about 1-km diam within a distance of about 100 m behind the rocket, and there is no appreciable change in rocket velocity within the 33 ms of the video frame. Therefore, any density change can be neglected.

Table 2 lists the physical, chemical, and performance properties of a typical Antares II thruster. Its propellant is poured around a central void shaped like a cylinder with four slots extending outward into the propellant; the slots lie in two planes passing through the central axis with 60–120–60–120-deg spacing. During flight the measured thrust and mass flow rate varied over a range that was 23% of maximum thrust; appropriate corrections were made in the analyses to follow. Experience with similar aluminized-solid formulations has shown that, in addition to the major species, measurable amounts of AlO, Al_2O, HCl, AlCl, $AlCl_3$, and OH vapor, as well as trace amounts of other gases, may be exhausted.[6] Some of these trace molecules can be expected to be hydrated or weakly chemically bonded to other exhaust species.

Figure 3 describes the ambient atmosphere for the geophysical conditions of the flight. Kinetic temperature, atomic-oxygen density, and total density (all atmospheric species) for the altitude range over which the Antares motor burned and smoldered were computed from the MSIS model.[13] The predicted concentration of the reactive $O(^3P)$ atoms varies by a factor of less than 2 over this altitude range. Collision mean free paths at these lower-thermosphere altitudes are much less than the characteristic dimensions of the radiating volumes, so continuum flow conditions exist.

Quantitative Results

Antares Burn

Figure 4 compares a set of transverse profiles (normalized to fixed camera gain) at four different times after Antares ignition; in each case the profile was measured at the location that Antares had passed through 3.0 s earlier. Two of these locations (for the 5- and 11-s

Table 2 Characteristics of the ANTARES II (X259A6) rocket engine

Dimensions,[a] cm	
Length (including exit cone), diam	289, 76.5
Throat diam	16.94
Propellant[a]	
Weight (0.91 of thruster motor), kg	1167
Composition, percent by weight	
Fuel (aluminum)	20.6
Oxidizers, binders, etc.	79.4
Heat of explosion (calculated), cal/g	1642
Exhaust (calculated)[a]	
Temperature (chamber), K	3760
Average mass flow rate, kg/s	33.3
Mean molecular weight of gases, amu	19.7
Molecule exhaustion rate, per cm path	2.5×10^{21}
Composition, moles/100 g of propellant	
Al_2O_3 (particles)	0.367
CO	1.392
H_2	0.985
N_2	0.513
H_2O	0.171
HCl	0.060
CO_2	0.043
H	0.018
$AlCl_3$, AlCl, AlO, Al_2O, AlO_2,OH	See text
Performance (see text for further detail)	
Duration of burn, s	35
Average thrust (measured, to 35 s), kgf	9370
Exhaust velocity, km/s	2.8[b]

[a]Manufacturer's data: Hercules, Inc., Cumberland, MD, 1966.
[b]Compare the rocket velocities in Table 1.

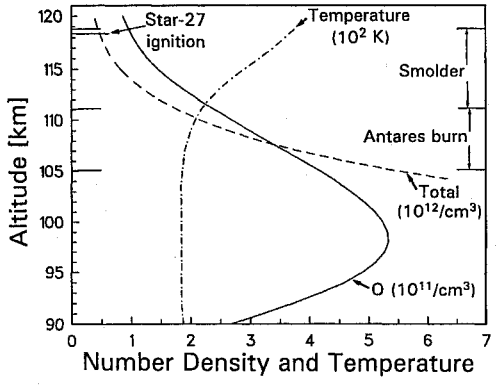

Fig. 3 Species concentrations and temperature of the ambient atmosphere.

profiles) are indicated in Figs. 2b and 2c (images taken 8 and 14 s after ignition). The altitudes were between 105.8 and 110.9 km. Absolute radiometric calibrations were too poor to permit useful quantitative comparisons of the total yield rates per unit path (the areas under these curves).

Figure 5 shows the relative intensity as a function of distance behind the rocket at five different times after ignition. Each curve is derived from a separate image, but the instrument gain did not change between images. A point on any curve represents the integration of a transverse profile (like those of Fig. 4); successive profiles advanced down the trail in steps of one horizontal pixel. (The broad peak in the 35.0-s curve is due to video blooming caused by intense radiation from Al_2O_3 particles.) The relative intensity at each location along the trail can be seen to decrease with time, indicating that the radiation is decaying at all altitudes, at least along this part of the trail. The curve for 37 s after ignition has been converted and replotted in Fig. 6, as follows: curve A results from the subtraction of background and the conversion of the abcissa from position (in the image) to time after Antares passage; curve B results from dividing curve A by the undisturbed local concentration of atomic oxygen. (We expect that atomic-oxygen density is the rate-limiting factor in the chemiluminescence of the exhaust gas.) The decrease in integrated intensity (curve B) is consistent with an exponential decay,

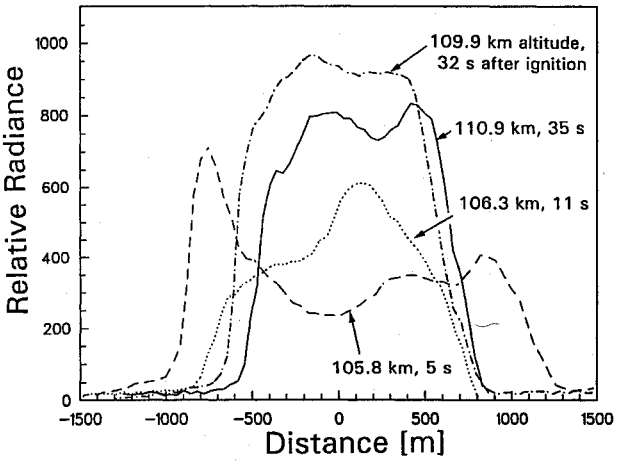

Fig. 4 Transverse radiance profiles 3 s after passage of the Antares engine.

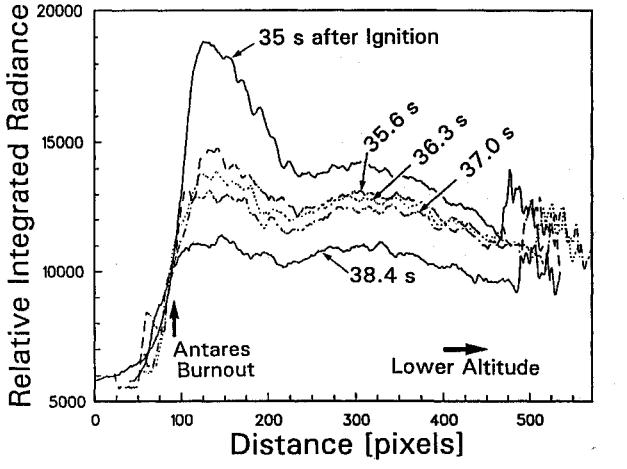

Fig. 5 Transversely integrated radiance as a function of distance along the Antares exhaust trail.

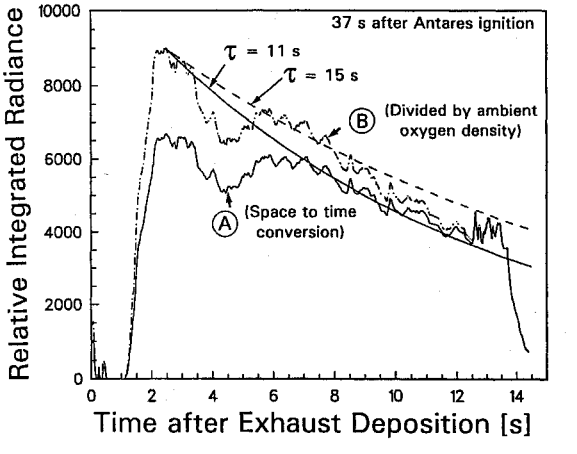

Fig. 6 Transversely integrated radiance as a function of time after deposition.

as shown by comparison with the 11- and 15-s pure exponentials. (These noisy data can, of course, also be fitted by other functional forms, including a straight line.) This value of 11–15 s is taken as the mean characteristic decay time of the total integrated intensity of visible light per unit distance over the 108- to 111-km altitude range in the first 14 s after passage of the rocket.

The frame 2 s earlier (35 s after ignition; Fig. 2d) was similarly analyzed. Figure 7 shows the integrated intensities for traces across the burn trail at four locations, corresponding to deposition times as much as 13.3 s after rocket passage, as well as one trace across the smolder trail (see Fig. 2e). These intensities gave a best-fit time

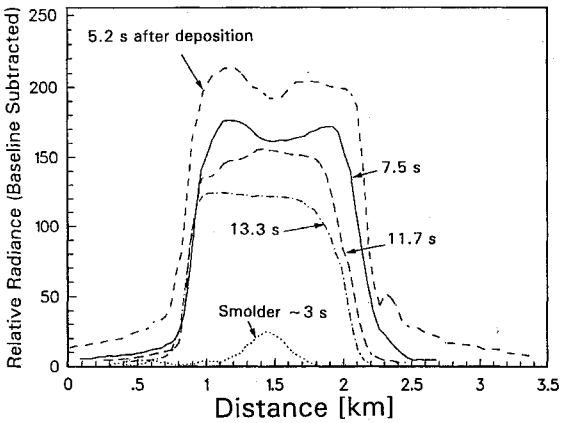

Fig. 7 Transverse radiance profiles at four locations on the Antares burn trail and one on the smolder trail.

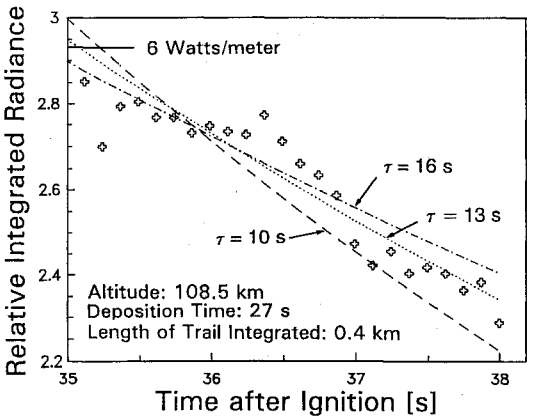

Fig. 9 Observed decay of the spatially integrated radiance within the box drawn in Fig. 2e.

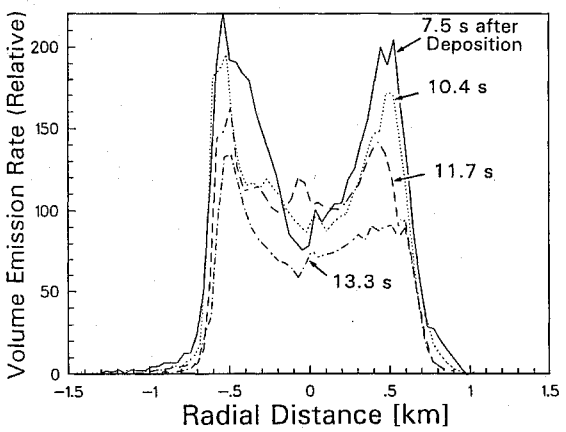

Fig. 8 Volume emission profiles obtained from Abel inversions of the radiance profiles.

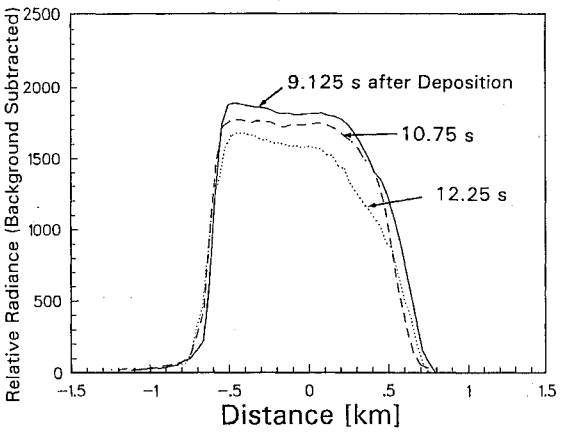

Fig. 10 Transverse radiance profiles at a fixed altitude of 108.2 km over an interval of 3.5 s.

constant of 13 s, in agreement with the preceding result. Figure 8 shows the radial dependence of volume emission rates derived from the radiance profiles (some from Fig. 7) by the method to be described.

We also determined this initial decay time by a second method. After Antares burnout, automatic tracking stopped briefly, the telescope remaining motionless for about 3 s and staring at the same location (the box drawn in Fig. 2e), so the decrease in intensity over about 90 frames was recorded. Figure 9 shows the intensity as a function of time; the best-fit time constant from these data is 13 s, in agreement with the result obtained over a wider range of altitudes. The box includes altitudes from 108.0 to 108.4 km.

The first method depends on the assumption that the intensity is proportional to the atomic-oxygen density, while the second does not. That both methods yield the same decay times suggests that the assumption is valid and that atomic oxygen (or another atmospheric species with a similar scale height) is a reactant in the chemiluminescence.

The visible-light power radiated at 108.2 km (8 s after exhaust deposition) is 6 kW per kilometer of trajectory path. If the decay continues with a time constant of 13 s, the total output is 140 kJ/km. This may be compared with the total thruster energy of about 200 MJ/km (10^{10} J expended over a flight path of about 50 km); the efficiency with which chemical energy is converted to visible photons at this altitude is 0.07%.

The series of traces in Fig. 7, taken from a single frame for 5.2–13.3 s after exhaust deposition (over a range of altitudes), shows little difference in the width of the radiating volume. Figure 10 shows transverse profiles (background subtracted) at a fixed altitude of 108.2 km over a 3.5-s period; again there is no significant change in trail width. We expect that the laterally expanded exhaust gas diffuses into the ambient air that it has initially compressed and heated (a simple transport-only model with no chemical consumption).[14] The effective diffusion coefficient would be two or three times the value of 2×10^6 cm^2/s for the undisturbed atmosphere at 108 km, and we expect that the size of the exhaust-gas cylinder increases by about 170 m in 3.5 s and 250 m in 8 s. However, the size of the luminous volume remains practically constant and confined to the boundary layer between the gas and the displaced atmosphere, which can be explained as follows. Neither the active exhaust constituent nor the atomic oxygen can diffuse very far into the other medium before reacting. The exhaust gases and the atmosphere are in fact diffusing into each other but are only luminous in the boundary layer. The boundary layer is the remnant of a shock created by the explosive expansion of gas leaving the rocket nozzle.[14]

By comparison with stars in the field of view, we find that the movement of the luminous volume perpendicular to the line of sight has a speed of 70 m/s, which is in the normal range for upper-atmospheric winds. This observation is added evidence that the radiation comes from a gas rather than micrometer-sized particles, which would not follow the wind field. Since a star can be seen through the glow volume (see Fig. 11), the trail must be optically thin over at least part of the visible spectrum.

On the basis of only one view direction and the assumption of simple growth symmetry, we presume the trail to be cylindrically symmetric. The relatively flat tops of the profiles of Figs. 7 and 10 show that the emission occurs mainly near the outer surface. This limb brightening can be seen directly in Fig. 8, which shows curves of volume emission rate per unit volume as a function of radial distance. These were derived by performing Abel inversions of the radiance profiles at 35 s; this treatment uses a half profile, assumes that the emission depends only on radial distance, and requires that the volume be optically thin to its own radiation. Since the inversion involves differencing, noise in Fig. 7 is amplified in Fig. 8, so depths of the troughs and widths of the edge regions are imprecise. Figure 11 is an isophote contour plot (with an absolute

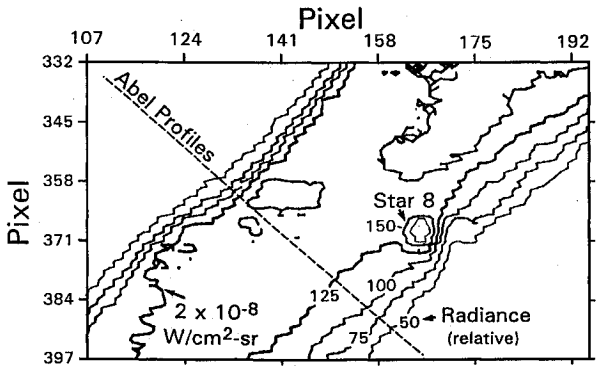

Fig. 11 Isointensity radiance contours in the region of the rectangular area indicated in Fig. 2e.

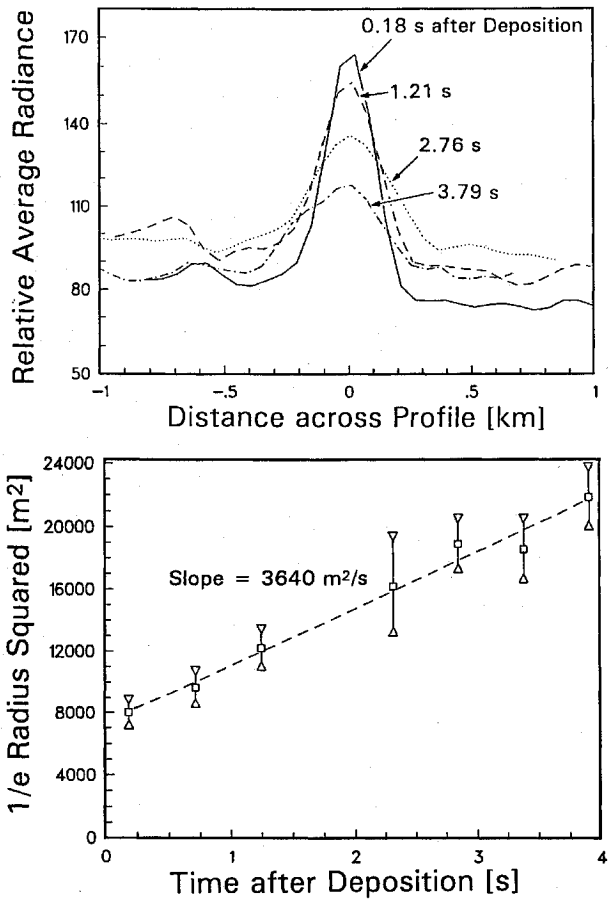

Fig. 12 Top panel: transverse radiance profiles of the Antares smolder trail at 114.5 km. Bottom panel: square of the trail radius as a function of time after deposition.

radiometric calibration) that includes the one-dimensional data used in one inversion.

Limb brightening is also apparent (Fig. 2a), during the first 16 s after ignition, in both the irregular and relatively smooth glow regions. The surface brightnesses in Figs. 7 and 10 exhibit less spatial modulation as the exhaust trail ages, and the peaks of high volume emission at the limb (Fig. 8) broaden and flatten. This damping and smoothing is expected from the characteristic diffusion coefficient estimated above; this value would be roughly the same for the exhaust gas and the air that it has displaced.

Antares Smolder

A similar analysis of the radiance during the interval after burnout when the Antares smoldered is summarized in Fig. 12. Using a bright star on each side of the trail as position references (see Fig. 2f at 49 s after ignition), we were able to stare for 3 s at a fixed 0.5-km segment of this trail, centered at 114.5-km altitude; the location is shown in Fig. 2f. Radiance profiles, shown in the top panel of Fig. 12, appear Gaussian-shaped even in the earliest frames, with a characteristic width that increases with the square root of time. The bottom panel of Fig. 12 shows trail radii (squared), as measured at $1/e$ of maximum intensity in the profiles of the top panel. The dashed line is a least-squares straight-line best fit; the error bars represent 1σ error from a regression analysis. If we apply the theory for diffusion of a reacting (or inert) species into a uniform, isothermal, undepleted atmosphere,[15] the slope of the dashed line leads to a diffusion coefficient of $(9 \pm 2) \times 10^6$ cm^2/s, which is roughly three times the small-molecule diffusion coefficient in the undisturbed atmosphere.[16] This factor of 3 is most likely due to the initially high mean temperature of the exhaust gas and surrounding air.[14] An extrapolation to zero (explosion) time, following the procedure developed for analyzing the growth of chemical-release clouds,[15] gives an initial Gaussian full width of 0.18 km. The decay time of the total emission rate per unit trajectory path is 3.5 ± 1.0 s, which is a factor of about 4 smaller than the time derived for the burn period, despite the fact that the concentration of atomic oxygen at this altitude is lower by a factor of almost 2. This difference is explained by the hydrodynamics to be discussed.

A comparison between the burn and smolder periods was made in the following way. Two transverse traces of Fig. 7 were used: the trace just before burnout (5.2 s after deposition) and the trace just after burnout (labeled "smolder"; 0.9 s after deposition). They were first integrated across the trail to obtain a value for total yield per unit length of the trail. An exponential decay curve with the appropriate time constant (13 and 3.5 s, respectively) was then drawn through each point, and the total area under each curve was taken as an estimate of the total time-integrated yield per unit trail length. The yield for the smolder just after burnout is smaller than the yield for burn just before burnout by a factor of 19. The profile just after burnout is roughly Gaussian (as it is in Fig. 12, 12 s later and 3.4 km higher), in contrast to the limb-brightened profile that characterizes the burn period.

Star-27 Burn

The solid-propellant third-stage Star-27 motor has about one-fourth as much thrust as the Antares. It is very similar to the Antares in terms of propellant and exhaust-product fractions. Like Antares, this stage also left a persistent glowing trail that was uniform in diameter but less bright. Unlike Antares, this motor did not produce a bright cloud at the point of ignition, presumably because its velocity was already quite high (2.5 km/s) so the deposition rate per unit trail length did not have a very high initial value. Because of the higher velocity, the trail moved out of the field of view too quickly (within about 1 s) to permit a quantitative determination of decay time, but it appears to be substantially longer than the 3.5 s found for the lower-altitude Antares smolder.

Figure 13 shows three transverse intensity profiles at an altitude of 118.5 km. Within the limited observation time, no lateral growth is apparent, as was the case for Antares. Abel inversions (not shown) of these noisy traces show a relatively flat volume emission rate, with a small amount of limb brightening.

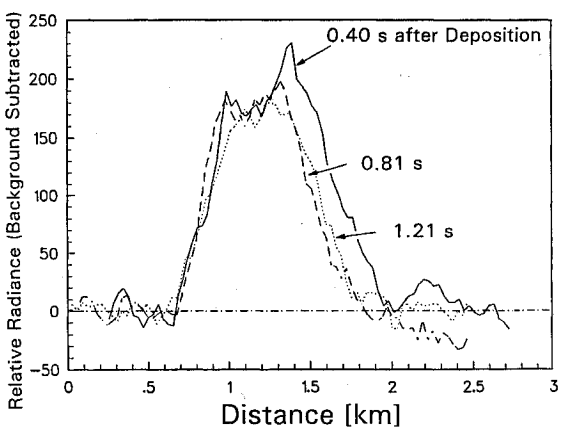

Fig. 13 Transverse radiance profiles of the Star-27 burn trail at 118.5 km.

Source of the Emission

Possible Excitation Mechanisms

Thermal (graybody) emission from the micrometer-size Al_2O_3 particles of the rocket exhaust cannot be responsible for the persisting visible luminosity. (As noted earlier, this emission was, in fact, observed spectroscopically very close to the exhaust nozzle.) First, such particles would expand much more slowly and would not produce an apparently stationary glowing surface. Second, these droplets cool in a fraction of a second to temperatures at which visible radiation would be negligible, as straightforward radiative-loss calculations show. An explanation of the emission in terms of chemiluminescent reactions occurring on the particle surfaces (e.g., recombination of atomic oxygen) is similarly ruled out because of the observed expansion characteristics.

We therefore consider the mechanism of chemical reactions of one exhaust species (cooled by expansion) with other exhaust or atmospheric molecules. Arguments against reactions between two exhaust species are, first, that no visible chemiluminous reaction is known to proceed significantly at the temperature of the combustion gas (less than 1000 K)[14] and, second, that the spatial distribution of such reactions would not produce the observed limb brightening, since the exhaust-gas density is lower at the limb.[14] The latter argument, as well as the fact that an altitude dependence was observed, also rules out a metastable exhaust species as the source of the emission. Consequently, we suggest that the emission results from the reaction of an exhaust product with an atmospheric species such as the highly reactive atomic oxygen. The reacting species may be either one of the major combustion products (see Table 2) or a trace constituent. Chemiluminescent reaction of atomic oxygen with an aluminum-containing product from a smoldering solid-propellant motor was advanced previously by O'Neil et al.[17] to explain a similar glow produced by a Hydac booster (5700-kgf thrust) as it reached an altitude of about 88 km.

Exhaust Transport and Scaling

To consider the hypothesis of chemiluminescence in greater detail, we need information about the spatial distribution of the likely reactants. Several hydrodynamic and kinetic models dealing with high-altitude chemical explosions,[14] photographic observations of aluminized grenades,[18] and gas releases in space[19] provide such information. A Rankine–Hugoniot shock forms when the ratio of $(E/P)^{1/3}$ to the collision mean free path goes above a critical value. The energetic self-colliding gas, in which density and temperature decrease outward, sweeps out (and so heats) virtually all the air in a volume that is proportional to E/P. After this initial expansion the transport of the explosion and atmospheric gases is diffusive. In spherically symmetric blasts[14,20] the radius of this volume, after a few strongly damped oscillations, reaches $0.21(E/P)^{1/3}$. For example, when 18 kg of RDX-Al-$CsNO_3$ (RDX is cyclotrimethylenetrinitramine) was exploded at 108.7 km in experiment Firefly Jeannie,[14] the measured radius was in agreement with the theory. (The radius, taken to be $2^{-1/2}$ times the stationary width of a decaying Gaussian density profile of constant total area, was 0.47 km, and the energy released by the explosive was 3.3×10^6 J/kg.) With less explosive or greater altitude, the shock becomes thicker, which increases the fraction of the explosion gas that is mixed with the atmosphere, thereby affecting the rate of chemiluminescent reaction.

The continuum-flow models of Groves[14] and Brode[20] can be extended to the case of the rocket trails by considering the motor burn as a line explosion with cylindrical symmetry, that is, an infinite number of explosions with infinitesimal spacing along the line of the trajectory. Since the explosion at each point along the trail is affected by the preceding and following points, this method is an approximation. (The rocket exhaust most closely resembles a line charge when the rocket speed greatly exceeds the outward-expansion speed.) In this approach, which has been used to analyze weaker explosions at higher altitudes,[21] the cylindrical geometry leads to the radius of the trail being proportional to $(\Lambda/P)^{1/2}$. When we apply this method to the Antares burn between 108.2 and 110.9 km, taking into account both the change in ambient pressure and a measured decrease in motor thrust over this 25–35-s period, we find that the calculated radius increases by about 15%. The radius values measured from the traces of Fig. 7 are consistent with this prediction but not sufficiently accurate to confirm it. Moreover, these profiles do not truly represent exhaust concentrations, since the emission arises only where mixing occurs.

The profiles of Fig. 4 (all 3 s old but covering a greater altitude range) are also consistent with this simple scaling rule to within the accuracy of the measurement. (The bifurcated trail just after ignition is an exception, since it results from nonsymmetrical burning.) More significantly, this scaling rule correctly predicts the radius of the Star-27 trail (lower energy and higher altitude) relative to the Antares trail.

In Figs. 4 and 7 we defined the measured boundary between the two gases to be the intersection of the baseline with the lines tangent to the steep segments of the radiance profiles. We determined the factor k in the equation for radius, $R = k(\Lambda/P)^{1/2}$, from the measured or known values; the observed mean values of k for the Antares (108.2–110.8 km) and for Star 27 (118.5 km) are 0.21 and 0.19, respectively. The agreement between these two values is satisfactory, considering the uncertainties in radius measurement, energy deposition rates, and atmospheric pressure. The fact that these values also agree with the value of 0.21 observed in spherically symmetric blasts[14] supports the idea that the phenomenon can be treated as a cylindrically symmetric line explosion. (In theory, the factor for spherical geometry should be 14% smaller than the factor for cylindrical geometry.)

Extension of this scaling principle to the Antares smolder is uncertain because 1) the energy deposition rates are hard to estimate and 2) the radius, not much larger than the diffusion length, is not well defined. If we assume that the ratio of ejected mass (glow-producing reactant) to thrust is the same before and after burnout, the exhaust deposition rate can be estimated from the measured emission rates and lifetimes. We further assume that the smolder is not an explosion, in the sense that a well-defined boundary between exhaust and atmosphere is not formed; therefore, the radiation decay time is determined mostly by chemical consumption throughout the volume rather than fluid-flow characteristics at a boundary. Then, if the residual thrust remains the same as at 111 km, the ratio Λ_s/Λ_b during the smolder (at 114.5 km) and the burn (at 108.2–110.8 km) is given approximately by 1/19 (integrated-brightness ratio) times 3.5/13 (decay-time ratio). Following the procedure described by Golomb and MacLeod,[15] we adopt the intercept on the ordinate in Fig. 12 (bottom panel) to define the pressure-equilibration radius; if we use this radius in the earlier equation $R_s = k(\Lambda_s/P)^{1/2}$, a value of 0.17 is obtained for the proportionality constant k. The rough agreement of this value with that derived above for the full-thrust burn may be somewhat fortuitous, since it is based on several weak assumptions. The emission profile of the smolder (a much weaker explosion) almost immediately exhibits a rounded profile because the shock is many collision mean free paths thick[14,19]; in contrast with the engine burn, all of the smolder exhaust quickly mixes with the atmosphere. A further caveat is that this proportionality constant may not apply to solid-composite motors with different chemical composition and grain configuration, which might exhibit different residual thrusts and fractions of light-producing exhaust species. Even individual Antares motors are known to vary significantly.

The rounded finger that extends backward just after Antares ignition is due to high-pressure exhaust gas expanding along the thrust axis into undisturbed air at or near ambient sound speed. The gas is confined radially by the air it has compressed. We ascribe the initial shape of the glowing cloud to the internal shape of the propellant (no cylindrical symmetry but mirror symmetry in four quadrants). The bumpy surfaces of this cloud move outward at much less than molecular-diffusion speeds because, like those of the subsequent trail, they are being chemically eroded.

Chemiluminous Reaction

Having concluded that the emission is produced by a chemiluminous reaction, we must look for one or more reactions of an exhaust species that are compatible with the following observations: 1) The chemical-consumption lifetime of the exhaust species is about 3.5 s at 114.5 km (where the smolder gases can be considered mixed with the atmosphere); if the ambient reactant is O, this lifetime would

require a bimolecular rate coefficient of about 1.5×10^{-12} cm^3/s [reciprocal of $(2 \times 10^{11}/\text{cm}^3) \times 3.5$ s]. 2) Column emission rates during the burn are about 10^{-8} W cm^{-2} sr^{-1} (Fig. 11; about 2×10^{11} photons cm^{-2} s^{-1} column^{-1}), which implies an outer-annulus volume emission rate near 5×10^6 photons cm^{-3} s^{-1}.

A review of the chemiluminous reactions of the principal combustion species with oxygen and nitrogen failed to identify any that are sufficiently fast to meet the first criterion. The reaction of minor species C_2O with O to produce CO(A-X) fourth positive bands has been invoked to explain the vacuum-ultraviolet radiation associated with a smoldering Aries solid-rocket booster.[22] However, this process could not be the source of the persisting glow in view of 1) the rapid consumption of C_2O (the rate coefficient at 300 K is 10^{-10} cm^3/s), 2) the low branching ratio to the upper states of visible emissions (about 10^{-5}), and 3) the expected very small concentration of C_2O in the Antares and Star-27 exhausts.

By contrast, some aluminum-containing molecules are known to react with oxygen in both the atmosphere[18,23] and laboratory[24,25] to produce closely packed electronic bands, which resemble a continuum. Visible radiation with a persistence in the range 2–100 s was observed when aluminum in three different forms was introduced into the atmosphere between 90 and 200 km at night: 1) the release of trimethyl aluminum [$Al(CH_3)_3$], 2) the burning of a mixture of $CsNO_3$ and aluminum powder (in effect, miniature solid-composite rocket motors), and 3) the explosion of aluminum-containing grenades (control TNT/RDX grenades without Al granules produced no glow). In the case of the aforementioned Hydac rocket motor, the decay time of the chemiluminescent wake was 1 s at 108 km and 0.5 s at 102 km (as estimated from the uncalibrated images reported by O'Neil et al.[17]). One possible conclusion[24] from these field experiments and supporting laboratory investigations is that the upper state(s) of the broad pseudocontinuum is excited in a substitution reaction: $XAlO + O \rightarrow AlO_2(^1B_2) + X$. The weakly coupled adduct X may be H_2O (Ref. 25); other candidates are H, OH, Cl compounds, or even another AlO molecule. The rate coefficient for the substitution reaction exceeds 10^{-13} cm^3/s (as this reaction may not be the rate-limiting step in the chain(s) producing the luminescence), which is in qualitative agreement with the figure derived in observation 1 above.

If we estimate (by extrapolation from the visible spectrum) that an equal number of near-IR photons are emitted, the mean initial number density of XAlO is $4 \times 10^7/\text{cm}^3$ (2 times 5×10^6 photons cm^{-3} s^{-1} times the 3.5-s decay time). This approximate figure (from observations 1 and 2 above) represents 0.02% of the exhaust molecules, which is in the range expected for trace species (such as XAlO) from the rocket motor. Since the density of reactant required to produce the observed emission is much less than the density of ambient O (Fig. 3), it is likely that reactant depletion limits the process. The densities of minor atmospheric species (such as O_3) are not sufficient to produce the measured intensities. Additionally, even if the column densities of ground-state AlO_2 were two or three orders of magnitude higher than those resulting from radiative decay of $AlO_2(^1B_2)$, the exhaust volumes would remain optically thin to their multiple overlapping band radiations.

Other possible light-producing reactions[26] are $Al + H_2O \rightarrow HAlOH^*$ and $AlX + O \rightarrow AlO^* + X$. The first (radiation-stabilized) reaction is exothermic by 3.4 eV and produces a continuum very similar in nature to AlO_2^*; it requires that Al atoms be produced at the surface of the trail to create the limb enhancement. Any atomic-oxygen-consuming reaction of the type $AlX + O \rightarrow Al + XO$ is feasible as this necessary precursor reaction. The second reaction has also been shown to be consistent with the properties of the chemiluminescence observed following injections of Al and Al compounds into the thermosphere.[26] Discovering which one (or more) of these reactions is responsible will require further data, such as spectroscopic measurements of the emission.

Concluding Comments

We have presented evidence that the persisting glow from the exhaust trail of a solid-propellant rocket is caused by chemiluminescent reactions with the ambient atomic oxygen of a minor exhaust species. Based on our review of related experiments, we have identified AlO_2, AlO, and (with less confidence) HAlOH as the species most likely responsible for the chemiluminescence. From our quantitative analysis of the visible emission, the fractional concentration of this minor species is 2×10^{-4}. Its efficiency for producing visible and short-wavelength infrared photons is about 0.0015, which is plausible in view of the multiplicity of channels possible for the species. Absolute visible brightness and emission rates per unit axial length of the trail have been determined. We have shown that the lateral dimension of the trail scales with the power output of the rocket and the ambient atmospheric pressure. The volume emission was shown to be greatest near the outer edge of the trail (limb brightening).

The decay time of the trail radiance is controlled by diffusion of the ambient oxygen back into the trail volume after having been swept out and compressed into a cylindrical shell by the initial expansion. Visible emission rates decrease exponentially with lifetimes of about 10 s. However, since the decay is strongly dependent on the density and pressure of the ambient oxygen, these lifetimes will vary substantially with geophysical conditions. Much later, when the exhaust and atmosphere are well mixed, the lifetimes will be smaller by roughly an order of magnitude (as in the case of the smolder trail).

We have sought to explain these experimental results in terms of a simple model. The long-term goal, however, may be to develop and validate a more detailed calculation that couples hydrodynamics and chemical reactions.

Acknowledgments

The authors thank M. A. MacLeod and R. Viereck of the U.S. Air Force Phillips Laboratory for useful discussions of the dynamics of gases released in the upper atmosphere, and N. Bennett and D. Kenny of PhotoMetrics, Inc., for their help in preparing the manuscript.

References

[1]Murad, E., Knecht, D. J., Viereck, R. A., Pike, C. P., Kofsky, I. L., Trowbridge, C. A., Rall, D. L. A., Ashley, G., Twist, L., Elgin, J. B., Setayesh, A., Stair, A. T., Jr., and Blaha, J. E., "Visible Light Emission Excited by Interaction of Space Shuttle Exhaust with the Atmosphere," *Geophysical Research Letters*, Vol. 17, No. 11, 1990, pp. 2205–2208.

[2]Broadfoot, A. L., Anderson, E., Sherard, P., Knecht, D. J., Viereck, R. A., Pike, C. P., Murad, E., Elgin, J. B., Bernstein, L. S., Kofsky, I. L., Rall, D. L. A., Blaha, J., and Culbertson, J., "Spectroscopic Observation at Wavelengths Near 630 nm of the Interaction Between the Atmosphere and the Space Shuttle Exhaust," *Journal of Geophysical Research*, Vol. 97, No. A12, 1992, pp. 19,501–19,508.

[3]Pickett, J. S., Murphy, G. R., Kurth, W. S., Goertz, C. K., and Shawhan, S. D., "Effects of Chemical Releases by the STS-3 Orbiter on the Ionosphere," *Journal of Geophysical Research*, Vol. A90, No. A4, 1985, pp. 3487–3497.

[4]Hermance, C. E., "Solid Propellant Ignition Theories and Experiments," *Fundamentals of Solid Propellant Combustion*, edited by K. K. Kuo and M. Summerfield, Vol. 90, Progress in Astronautics and Aeronautics, AIAA, New York, 1984, pp. 241–304.

[5]Price, E. W., "Combustion of Metallized Propellants," *Fundamentals of Solid Propellant Combustion*, edited by K. K. Kuo and M. Summerfield, Vol. 90, Progress in Astronautics and Aeronautics, AIAA, New York, 1984, pp. 479–513.

[6]Shorr, M., and Zahringer, A. J. (eds.), *Solid Rocket Technology*, 1st ed., Wiley, New York, 1967, p. 327.

[7]Sutton, G. P., *Rocket Propulsion Elements*, 6th ed., Wiley, New York, 1992, p. 197.

[8]Pike, C. P., Knecht, D. J., Viereck, R. A., Murad, E., Kofsky, I. L., Maris, M. A., Tran, N. H., Ashley, G., Twist, L., Gersh, M. E., Elgin, J. B., Berk, A., Stair, A. T., Jr., Bagian, J. P., and Buchli, J. F., "Release of Liquid Water from the Space Shuttle," *Geophysical Research Letters*, Vol. 17, No. 2, 1990, pp. 139–142.

[9]Smathers, H. W., Horan, D. M., Cardon, J. G., Malaret, E. R., Singh, M., Sorensen, T., Laufer, P. M., Corson, M. R., Brandenburg, J. E., McKay, J. A., and Strunce, R. R., Jr., "Ultraviolet Plume Instrument Imaging from the LACE Satellite: The Strypi Rocket Plume," U.S. Naval Research Lab., NRL/FR/8121-93-9526, Washington, DC, Sept. 1993.

[10]Candler, G., Levin, D. A., Brandenburg, J. E., Collins, R. J., Erdman, P. W., Zipf, E. C., and Howlett, C., "Comparison of Theory with Plume Radiance Measurements from the Bow Shock Ultraviolet 2 Rocket Flight," AIAA Paper 92-0125, Jan. 1992.

[11]Erdman, P. W., Zipf, E. C., Espy, P., Howlett, C., Collins, R. J., Christou, C., Levin, D. A., and Candler, G. V., "In Situ Measurements of UV and VUV Radiation from a Rocket Plume and Re-Entry Bow Shock," AIAA Paper 92-0124, Jan. 1992.

[12]Warren, W. H., Jr., "Documentation for the Machine-Readable Character-Coded Version of the SkyMap Catalogue," NASA, NSSDC/WDC-A-R&S 81-05, Greenbelt, MD, July 1981.

[13]Hedin, A. E., "MSIS-86 Thermospheric Model," *Journal of Geophysical Research*, Vol. 92, No. A5, 1987, pp. 4649–4662.

[14]Groves, G. V., "Initial Expansion to Ambient Pressure of Chemical Explosive Releases in the Upper Atmosphere," *Journal of Geophysical Research*, Vol. 68, No. 10, 1963, pp. 3033–3047.

[15]Golomb, D., and MacLeod, M. A., "Diffusion Coefficients in the Upper Atmosphere from Chemiluminous Trails," *Journal of Geophysical Research*, Vol. 71, No. 9, 1966, pp. 2299–2305.

[16]National Oceanic and Atmospheric Administration/NASA/U.S. Air Force, *U.S. Standard Atmosphere, 1976*, U.S. Government Printing Office, Washington, DC, 1976, p. 7.

[17]O'Neil, R. R., Bien, F., Burt, D., Sandock, J. A., and Stair, A. T., Jr., "Summarized Results of the Artificial Auroral Experiment Precede," *Journal of Geophysical Research*, Vol. 83, No. A7, 1978, pp. 3273–3280.

[18]Rosenberg, N. W., "Chemical Releases at High Altitude," *Science*, Vol. 152, No. 3725, 1966, pp. 1017–1027.

[19]Bernhardt, P. A., "High Altitude Gas Releases: Transition from Collisionless Flow to Diffusive Flow in a Nonuniform Atmosphere," *Journal of Geophysical Research*, Vol. 84, No. A8, 1979, pp. 4341–4354.

[20]Brode, H. L., "Blast Wave from a Spherical Charge," *Physics of Fluids*, Vol. 2, No. 2, 1959, pp. 217–229.

[21]Klein, M. M., "Similarity Solution for Cylindrical Gas Cloud in Rarefied Atmosphere," *Physics of Fluids*, Vol. 12, No. 5, 1968, pp. 964, 965.

[22]Frankel, D. S., Gersh, M. E., McIntyre, A., Huffman, R. E., and Paulsen, D. E., "Aries Rocket Motor Infrared and Ultraviolet Spent-Stage Emission," *Journal of Spacecraft and Rockets*, Vol. 22, No. 5, 1985, pp. 567–573.

[23]Rosenberg, N. W., Golomb, D., and Allen, E. F., Jr., "Chemiluminescence of Trimethyl Aluminum Released into the Upper Atmosphere," *Journal of Geophysical Research*, Vol. 68, No. 20, 1963, pp. 5895–5898.

[24]Golomb, D., and Brown, J. H., "Chemiluminescence of Trimethyl Aluminum in Active Oxygen and Nitrogen," *Combustion and Flame*, Vol. 27, No. 3, 1976, pp. 383–389.

[25]Oblath, S. B., and Gole, J. L., "On the Continuum Emissions Observed upon Oxidation of Aluminum and Its Compounds," *Combustion and Flame*, Vol. 37, No. 3, 1980, pp. 293–312.

[26]Gole, J. L., and Kolb, C. E., "On the Upper Atmospheric Chemiluminescent Emission Observed upon Release of Aluminum Vapor and Its Compounds," *Journal of Geophysical Research*, Vol. 86, No. A11, 1981, pp. 9125–9136.

I. D. Boyd
Associate Editor